Article:
Sun, W., Zhang, Y., Gregory, D.A. orcid.org/0000-0003-2489-5462 et al. (7 more authors) (2020) Patterning the neuronal cells via inkjet printing of self-assembled peptides on silk scaffolds. Progress in Natural Science: Materials International, 30 (5). pp. 686-696. ISSN 1002-0071

https://doi.org/10.1016/j.pnsc.2020.09.007

Progress in Natural Science: Materials International xxx (xxxx) xxx–xxx

HOSTED BY

ELSEVIER

Contents lists available at ScienceDirect

Progress in Natural Science: Materials International

journal homepage: www.elsevier.com/locate/pnsmi

Patterning the neuronal cells via inkjet printing of self-assembled peptides on silk scaffolds

Weizhen Sun[a], Yi Zhang[a], David A. Gregory[a,d], Ana Jimenez-Franco[a], Mhd Anas Tomeh[a], Songwei Lv[b], Jiqian Wang[c], John W. Haycock[d], Jian R. Lu[e], Xiubo Zhao[a,b,*]

[a] Department of Chemical and Biological Engineering, University of Sheffield, Sheffield, S1 3JD, UK
[b] School of Pharmacy, Changzhou University, Changzhou, 213164, China
[c] Centre for Bioengineering and Biotechnology, China University of Petroleum (East China), Qingdao, 266555, China
[d] Department of Materials Science & Engineering, University of Sheffield, Sheffield, S1 3JD, UK
[e] School of Physics and Astronomy, University of Manchester, Manchester, M13 9PL, UK

ARTICLE INFO

Keywords:
Neurobiology
Micro-patterning
Inkjet printing
Self-assembling peptides
PC12 cells

ABSTRACT

The patterning of neuronal cells and guiding neurite growth are important for neuron tissue engineering and cell-based biosensors. In this paper, inkjet printing has been employed to pattern self-assembled I_3QGK peptide nanofibers on silk substrates for guiding the growth of neuron-like PC12 cells. Atomic force microscopy (AFM) confirmed the dynamic self-assembly of I_3QGK into nanofiber structures. The printed self-assembled peptide strongly adheres to regenerated silk fibroin (RSF) substrates through charge-charge interactions. It was observed that in the absence of I_3QGK, PC12 cells exhibited poor attachment to RSF films, while for RSF surfaces coated or printed with peptide nanofibers, cellular attachment was significantly improved in terms of both cell density and morphology. AFM results revealed that peptide nanofibers can promote the generation of axons and terminal buttons of PC12 cells, indicating that I_3QGK nanofibers not only promote cellular attachment but also facilitate differentiation into neuronal phenotypes. Inkjet printing allows complex patterning of peptide nanofibers onto RSF substrates, which enabled us to engineer cell alignment and provide an opportunity to direct axonal development *in vitro*. The live/dead assay showed that printed I_3QGK patterns exhibit no cytotoxicity to PC12 cells demonstrating potential for future nerve tissue engineering applications.

1. Introduction

Peripheral nerve injuries account for 2.8% of all trauma injuries worldwide, which are typically the results of crush, penetration, traction, electric shock and vibration injuries [1]. These injuries affect millions of people worldwide resulting in a reduction of people's life expectancy as well as increasing social and economic burdens. Although injured nerves have the ability to regenerate, external therapeutic interventions are needed to ensure proper healing. Therefore, the development of engineered nerve scaffolds to guide neural cell attachment, alignment and proliferation has attracted significant attention [1–4].

However, fabricating scaffolds to direct neuron cell growth is challenging. Cell patterning is an important technology that enables researchers to accurately position populations of cells to designated areas on a substrate and promote the design of complex biological systems to study cell behaviour such as cell alignment, cell-cell interaction, cell-environment interaction, drug screening and cell based sensors [5–7]. In these applications, the chemical and topographical patterning of the systems become important factors that affect cell behaviour such as attachment and migration [8]. A technology that provides fast fabrication of patterned scaffolds/substrates allowing researchers to better understand cell behaviour and program the cell functions is therefore essential. Such studies will provide valuable information for future tissue engineering, drug screening and biosensor applications. Common techniques currently employed for surface patterning include lift off patterning, micro-contact printing and a variety of direct writing techniques, which are complex and expensive [9–13].

Polydimethylsiloxane (PDMS) and polyvinyl alcohol (PVA), are often used to provide patterns via lift-off patterning techniques [14]. Although such systems have the ability to modify mechanical, optical and chemical properties of the substrates, it requires complex steps (such as master moulds) and also high standard clean rooms [15,16]. In addition to this, the fabrication of master moulds for different patterns

* Corresponding author. Department of Chemical and Biological Engineering, University of Sheffield, Sheffield, S1 3JD, UK.
E-mail address: xiubo.zhao@sheffield.ac.uk (X. Zhao).

https://doi.org/10.1016/j.pnsc.2020.09.007
Received 25 April 2020; Received in revised form 11 September 2020; Accepted 13 September 2020

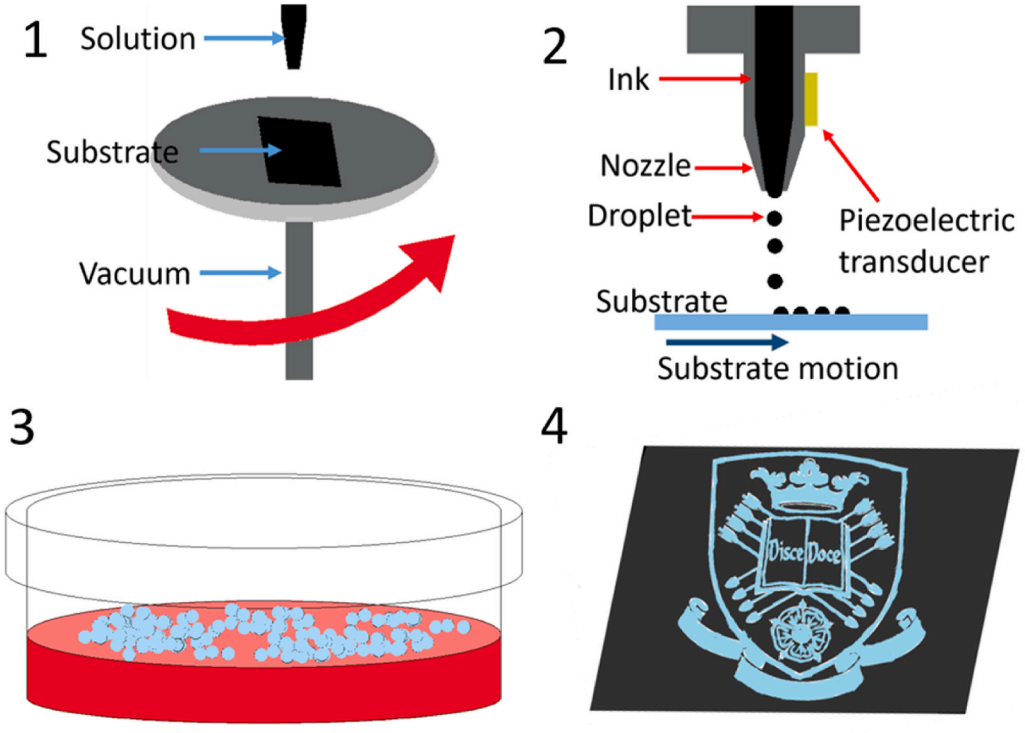

Scheme 1. A schematic diagram illustrating the fabrication of micro-patterns on RSF substrates via spin coating ad inkjet printing, as well as cell attachment on the surface of printed patterns.

is also very costly. Deposition of cell attractive substances [17] such as fibronectin [18], collagen [19], gelatin [20] or cell repelling agents such as wax [21] and polyethylene glycol (PEG) [22] onto a substrate is another approach for cell patterning. Such methods are normally combined with photolithography or chemical vapour deposition. For example, Ren et al. [12] deposited biotin-BSA onto glass with the help of photolithography and successfully patterned the cells into dot arrays. Wang et al. [13] have patterned a notch signalling ligand (Jagged1) and cell adhesion molecule (N-cadherin) using micro-contact printing to study cell-microenvironment and cell-cell interactions. However, such methods are costly, and the materials used are expensive. It is desirable to use cost-effective methods for patterning, with biocompatible and degradable materials for both attractive and repelling agents. Here, we use a self-assembled peptide as a cell attractive agent and regenerated silk fibroin (RSF) as a repelling agent to pattern neuronal PC12 cells by inkjet printing. Inkjet printing is a non-contact, cost effective, highly controllable and time saving technique that can print complex patterns (via CAD/BITMAP design) onto substrates. The particular strength of inkjet printing is its ability to precisely place pico-litres of ink at predetermined locations either side by side, or one on top of the other, resulting in 2D or 3D patterns/structures [23]. Multiple print heads also allow the rapid changeover of inks making it ideal for fabrication through reaction/crosslinking between different inks and also the incorporation of multiple components (e.g. different peptides and growth factors) during fabrication. It also enables fast and personalized fabrication at large scale. Silk fibroin (SF), a protein produced by silkworms during their pupation, is a well-known biomaterial, and many silk-based medical devices have been approved by FDA (Food and Drug Administration) [24,25]. In recent years, SF has been extensively used as a scaffold material for bone [26], vascular [27] and skin [28] repair due to its beneficial properties including excellent biocompatibility, biodegradability, low immunogenicity, high mechanical performance and commercial availability [29,30]. RSF solution has been used to produced many different types of scaffolds including gels [31], sponges [32], films [33] and fibres [34,35]. However, pure SF materials are known to have poor biological interactivity due to their inert properties (e.g. overall weak negatively charged and a lack of cell recognized peptide segments such as RGD), which normally manifests itself by a low cell binding efficiency, particularly to neuronal cells [36,37]. Therefore, addition of cell recognized moieties (e.g. poly-L-lysine [38], extracellular matrix (ECM) proteins [39]) is required to improve neuronal cell attachment and proliferation, ensuring its successful implementation as a scaffold biomaterial in neural tissue engineering.

ECM secreted by tissue or organs has been widely used in scaffold fabrication to provide a niche for tissue growth and regeneration [40,41]. Over the last two decades, it has been shown that active peptide sequences such as IKVAV, YIGSR and RGD in ECM can promote cell proliferation and attachment as well as promote neurite outgrowth [42–44]. For example, recently Motta et al. [45] reported on grafting a series of laminin-derived peptides to substrate surfaces with different concentration gradients and used them for the study of Schwann cell adhesion, proliferation and alignment with the concentration direction. It was found that Schwann cells displayed faster migration in the direction of the concentration profile. Self-assembly nanoscale fibrous scaffolds mimicking ECM have also been successfully employed in tissue regeneration [46]. The 'bottom-up' approach allows the fabrication of scaffold materials with well-ordered nanostructures [47,48]. For example, RAD16-I [49,50], RAD16-II [51], EAK16-I [52], EAK16-II [53] have been successfully used as hydrogel scaffolds for tissue engineering. Shorter self-assembling peptides have also been used for biomedical applications. For example, I_3QGK has been used for haemostasis in animal models with no immunogenic responses [54]. The peptide contains a hydrophobic tail made of three isoleucine residues (Ile or I) and a hydrophilic head group (QGK), and can form long and uniform nanofibers in aqueous solutions. The peptide self-organized itself with the tails inside the nanofibers to form a hydrophobic core and the hydrophilic head group on the outside of the nanofibers. The positively charged peptide exhibited excellent biocompatibility and can be potentially used for enhancing cell attachment and proliferation [54]. In addition, compared to neutral biomaterial, cationic biomaterial

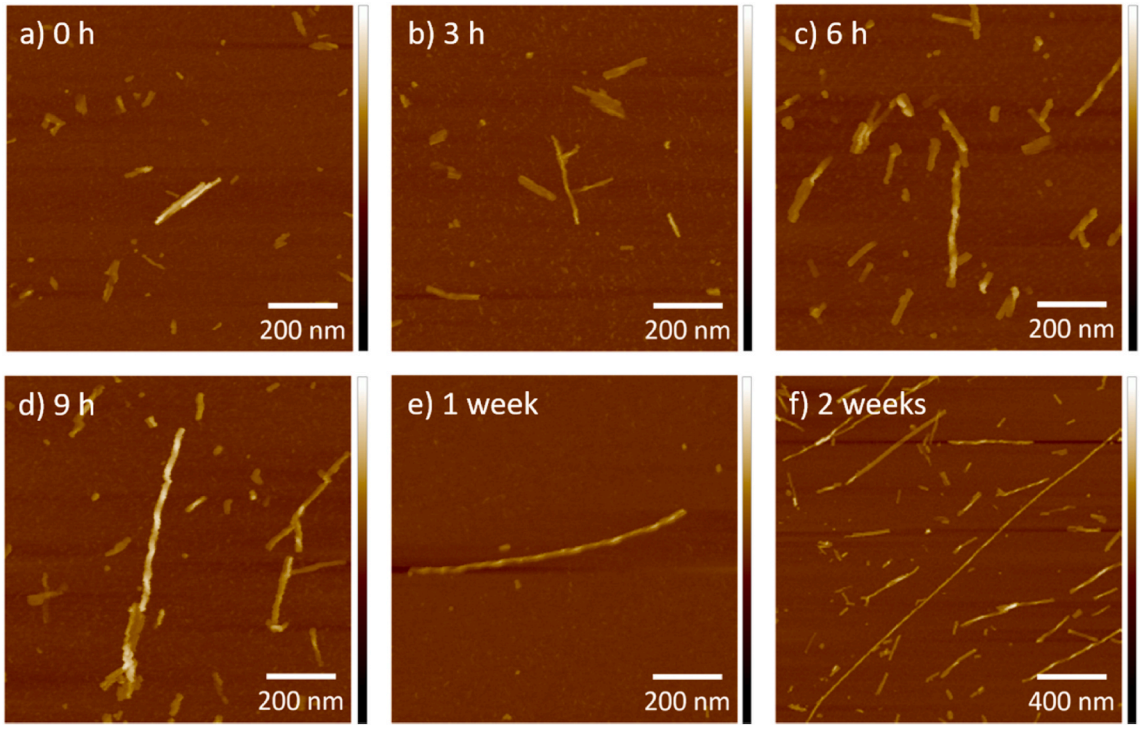

Fig. 1. AFM topographical images of I_3QGK dynamic self-assembly (1 mg/mL in 20 mM HEPES buffer at pH 6.0) at different time scales. (a) 0 h; (b) 3 h; (c) 6 h; (d) 9 h; (e) 1 week and (f) 2 weeks. The Z scales for all images = 30 nm as indicated. The self-assembly process of the peptide was a dynamic process. In the early stages (< 6 h), the peptides formed short stacks through hydrophobic interactions between the I_3 tails. Further growth of the stacks leads to formation of twisted fibres (> 6 h).

has been reported to causes less significant lysosome and DNA damage, as well as having a higher success rate in the self-repair of neural cells [55].

In this paper, self-assembled I_3QGK peptide nanofibers were patterned onto negatively charged RSF films [56] via spin coating and inkjet printing to guide cell attachment (Scheme 1). Rat pheochromocytoma neuronal (PC12) cells were then studied as an *in vitro* model for neuronal differentiation and neurite formation [57–59]. The cell attachment, viability and phenotype of PC12 cells on the patterned surfaces were investigated. The results demonstrate that inkjet printing is an effective method to pattern the scaffolds for guiding neural cell growth [60]. The technology has great potential to be used in the future for the fabrication of delicate scaffolds for neuron tissue engineering.

2. Experimental section

2.1. Materials

The *Bombyx mori* silkworm cocoons were provided by the state key laboratory of silkworm genome biology (Southwest University, China). The synthetic peptide AC-I_3QGK-NH_2 (> 98%, w/w) was purchased from GL Biochem Ltd. (Shanghai, China). PC12 Adh neuronal cells were obtained from HPA (Health Protection Agency) culture collections. Prior to each experiment the glass slides were immersed in 1 M HCl and 1 M NaOH for 1 h separately and then rinsed with deionized (DI) water before being dried using a compressed air line. Silicon wafers (Compact Technology Ltd, UK) were cut into 1 cm^2 and immersed in DI water for 1 day, then cleaned with 5% Decon 90 solution (Decon Laboratories Ltd, UK), before rinsing with copious amounts of DI water [61]. The reagents were purchased from Sigma Aldrich, UK.

2.2. Time effect of peptide self-assembly

The synthetic peptide I_3QGK was dissolved in 20 mM HEPES buffer (pH 6.0) at 1 mg/mL. 20 μL samples were taken at different time intervals over the course of two weeks (0 h, 3 h, 6 h, 9 h, 1 week and 2 weeks), and were dripped onto fresh mica and dried under ambient conditions prior to atomic force microscopy (AFM) characterization.

2.3. Atomic force microscopy

AFM (Bruker Dimension Icon, Bruker Corporation, USA) was used to characterize the topography of the coated samples and the cell morphology under ambient condition. The measurements were conducted in tapping model with SCANASYST-AIR probes. The images were analysed in NanoScope Analysis software (Version 1.5).

2.4. Preparation of regenerated silk fibroin (RSF)/peptide scaffolds

The silk cocoons were washed 3 times with hot DI water and boiled for 1.5 h in 0.02 M Na_2CO_3 solution before being rinsed 3 times with DI water to remove sericin. After being dried for 2 days at 60 °C in a drying oven, the degummed fibroin was dissolved in Ajisawa's reagent ($CaCl_2$/EtOH/DI water = 1:2:8 molar ratio) at 80 °C for 1.5 h. The solution was then dialyzed against DI water until the conductivity of DI water was below 10 μS/cm. Samples were then centrifuged for 10 min at 10,000 rpm. The concentration of the RSF solution was determined by weighing dried RSF peptide residues on microscope slides. The RSF solution was then stored at 4 °C prior to use.

The synthetic peptides were dissolved in 20 mM HEPES buffer (pH 6.0) at 5 mg/mL and incubated for 7 days at ambient conditions prior to use. The RSF was diluted with DI water to 40 mg/mL and peptide solutions were diluted with HEPES buffer (20 mM, pH 6.0) to 4, 3, 2 and 1 mg/mL.

RSF/peptide scaffolds were coated onto clean glass slides (cut to 1 cm^2) or silicon wafers sequentially via spin coating (Laurell Technologies Corporation, USA). The concentration ratios of RSF/peptides were 0:5 (peptide concentration 5 mg/mL, without RSF

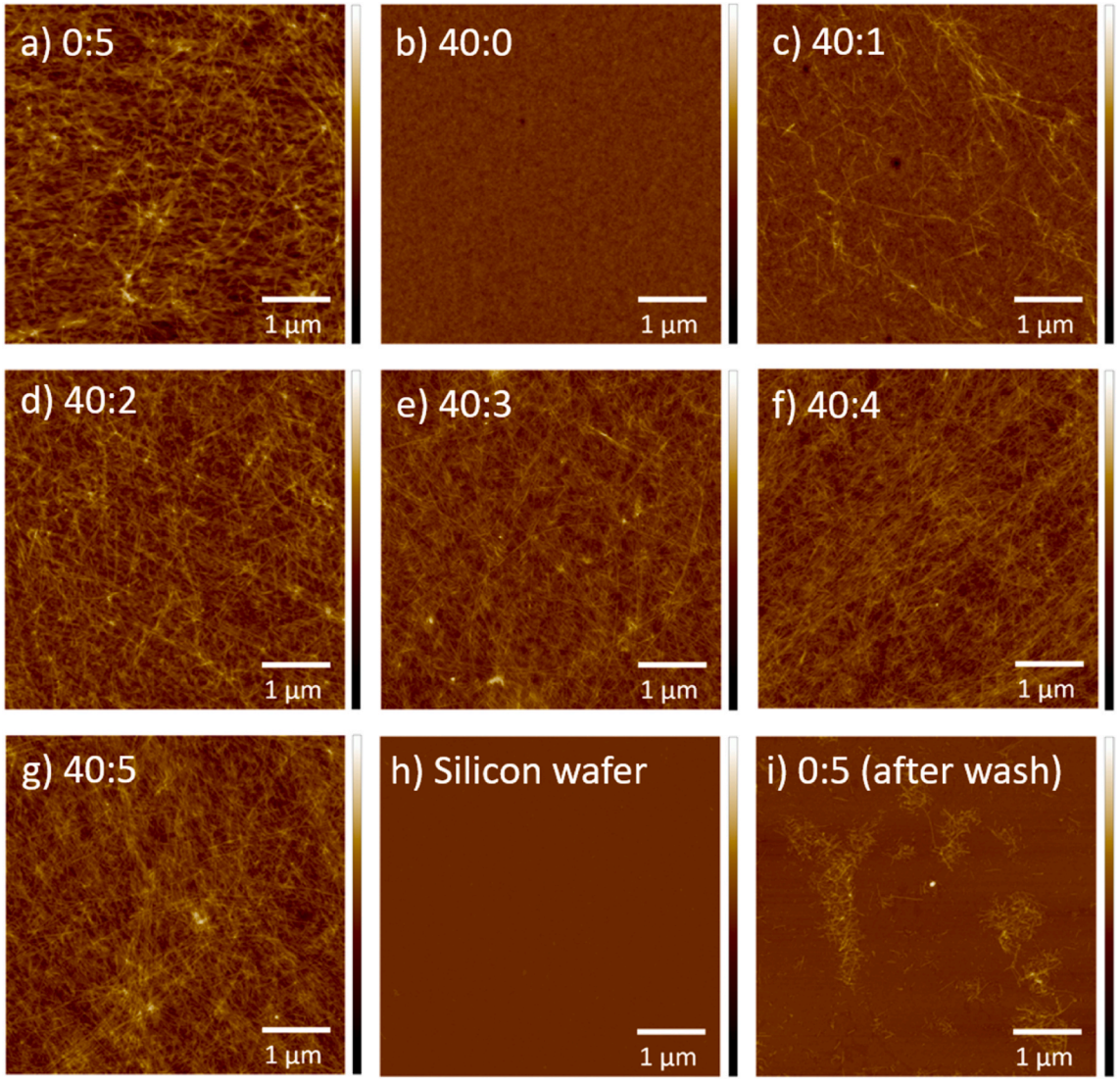

Fig. 2. AFM topographical images (25 μm^2) of RSF/I_3QGK scaffolds. RSF/I_3QGK scaffolds coated at different ratios: (a) 0:5 (only peptide), (b) 40:0 (only RSF), (c) 40:1, (d) 40:2, (e) 40:3, (f) 40:4, (g) 40:5, and (h) is an uncoated silicon wafer. (i) Shows the I_3QGK (5 mg/mL) coated glass surface after being washed with DI water. The Z scales (height) of all images are 60 nm.

precoating), 40:0 (RSF concentration 40 mg/mL, without peptide coating), 40:1, 40:2, 40:3, 40:4 and 40:5, respectively. For RSF/peptide bilayer samples, RSF solution (30 μL, 8000 rpm, 25 s) was coated followed by 95% ethanol solution (20 μL, 4000 rpm, 25 s), converting RSF into beta sheet conformation (silk II) [62]. Then, the peptide solution with the appropriate concentration was spin coated onto the substrates (30 μL, 8000 rpm, 25 s).

2.5. Surface patterning of self-assembled peptide using inkjet printing

Prior to printing, 1 layer of RSF solution (40 mg/mL) was coated on the glass slides (30 μL per cm^2, 8000 rpm, 25 s) followed by 95% ethanol solution (20 μL, 4000 rpm, 25 s) via spin coating. A Jetlab 4xL (MicroFab Inc., Texas, US) equipped with a piezoelectric drop-on-demand (DoD) printhead (60 μm nozzle diameter) was used for the printing of the I_3QGK peptide nanofibers (3 mg/mL aged for 1 week prior to use). The actuation voltage and frequency used were 90 V and 300 Hz respectively. The distance between the print head tip and the substrate was approximately 1 mm. To investigate the effect different patterns on the cell growth, straight lines and the university logo were printed. Lines were printed with varying number of layers of peptide (i.e. 1, 3, 5, layers).

2.6. Cell culture on scaffolds

Prior to use, the scaffolds were washed in phosphate buffered saline (PBS) and sterilized under ultraviolet light for 30 min. The samples containing RSF/I_3QGK scaffolds were placed in 12 well plates or petri dishes under metal rings (to secure the samples). PC12 neuronal cells were cultured in Dulbecco's Modified Eagle's Medium (DMEM) supplemented with 10% foetal calf serum (FCS), 1% penicillin, 0.5% amphotericin, and 1% glutamine at 37 °C under 5% (v/v) CO_2. The medium was refreshed every 3 days. Confluent cells were then detached with 0.25% (w/v) trypsin-EDTA and counted using a haemocytometer. The cells were seeded onto the samples with a seeding density of 10,000 cells/cm^2 and cultured for 2 days in DMEM medium containing 10% FCS and a further 4 days in serum-free medium.

2.7. Live/dead assay

A live/dead assay was carried out by replacing DMEM medium with serum-free medium containing 0.001% (v/v) Syto-9™ (Invitrogen) and

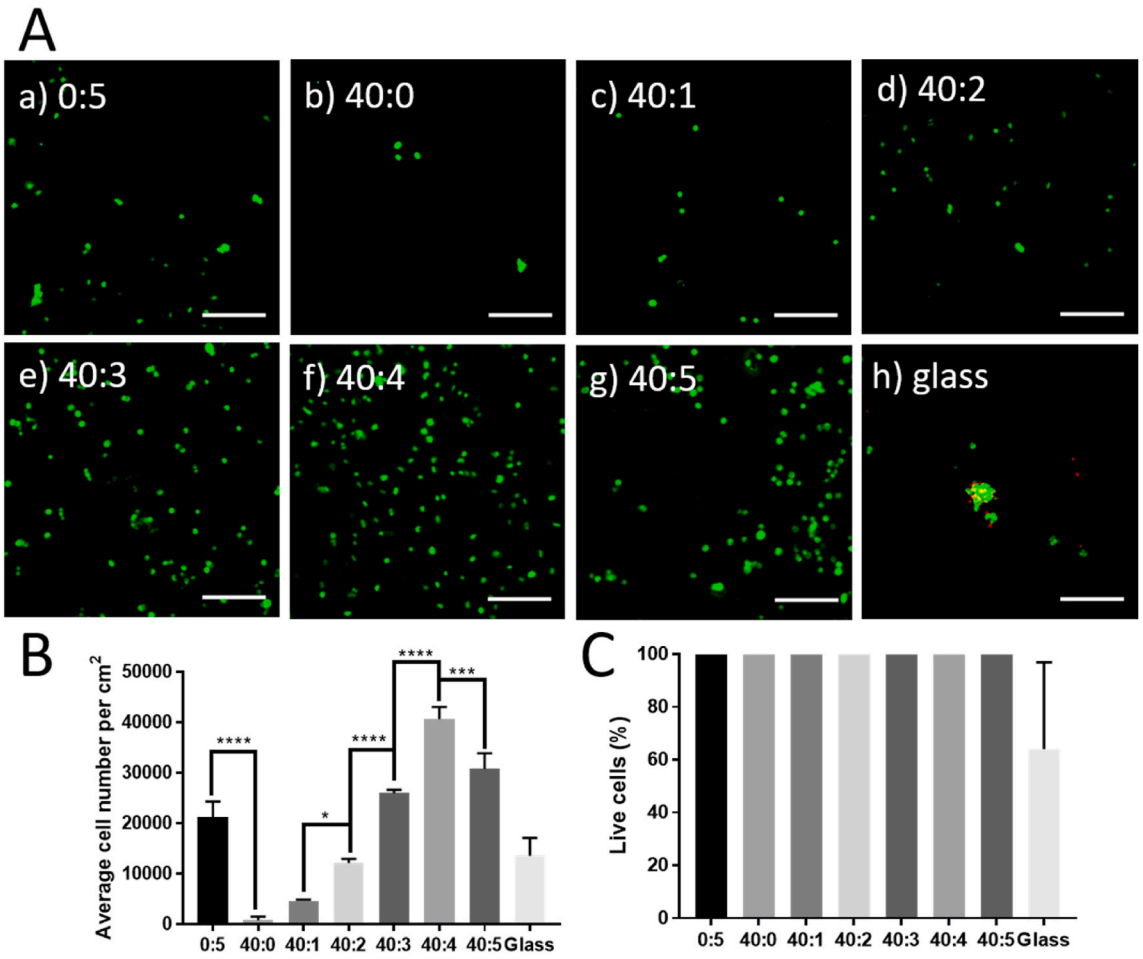

Fig. 3. A, Live/dead assay of PC12 neuronal cells on different RSF/I_3QGK coated substrates (green: live cells (Syto-9™ staining) and red: dead cells (propidium iodide staining). The concentration ratios for coating between RSF and I_3QGK were: (a) 0:5, (b) 40:0, (c) 40:1, (d) 40:2, (e) 40:3, (f) 40:4, (g) 40:5 and (h) glass control. Scale bars = 100 μm for all images. **B,** Average cell number (per cm^2) attached on various coated surfaces. **C,** Percentage of live cells on various coated surfaces ($n \geq 3$; ****$p < 0.0001$; ***$p < 0.001$; *$p < 0.05$).

0.0015% (v/v) propidium iodide (PI) before incubating for 30 min under a 5% CO_2 atmosphere at 37 °C. The cells were rinsed with PBS before being imaged under a fluorescence microscope (Nikon Eclipse LV100).

2.8. Cell counting

ImageJ analysis software was used to count the live and dead cells. The original image was converted to an 8-bit image and the threshold was adjusted to generate a high contrast binary image. Cells were then counted with the ImageJ 'analyse particles' algorithm for several images of 2500 μm^2 sample areas and averaged.

2.9. Phalloidin staining assay

Cells were fixed with 3.7% formaldehyde in PBS for 45 min at room temperature and then washed twice with PBS buffer and incubated for a further 45 min with 0.1% Triton X-100. The cells were then washed twice again with PBS buffer and the actin filaments were stained with phalloidin-FITC (λ_{ex} 494 nm/λ_{em} 520 nm) and nuclei were stained with DAPI (λ_{ex} 340 nm/λ_{em} 488 nm). The samples were then imaged using a fluorescence microscope (Nikon Eclipse LV100).

2.10. Statistical analysis

GraphPad Prism (7.04 version) was used to analyse the data quantitatively. One-way ANOVA (analysis of variance) with multiple comparisons was used for all multiple group experiments. The equality was confirmed by Tukey's multiple comparisons test. P values < 0.05 were considered significant.

3. Results and discussion

3.1. Time effect of peptide self-assembly

The dynamic self-assembly process of I_3QGK was similar to that of I_3K [63,64]. Small I_3QGK molecules aggregated through hydrophobic interactions between the I_3 tails within the first several hours (Fig. 1a and b) and formed bilayer stacks. Continued growth of the bilayer stacks was observed resulting in the formation of twist nanoribbons (Fig. 1c–e) due to molecular chirality and electrostatic repulsion. Long uniform nanoribbons with widths of 30 nm and heights of 5–10 nm were observed after 2 weeks incubation (Fig. 1f). The size of the nanofibers is consistent with the result reported by Chen et al. [54].

3.2. Characterization of RSF/I_3QGK scaffolds

The surface topography of the scaffolds has significant effect to the cell attachment. To establish the relation between the scaffold surfaces and the cell attachment, AFM was used to characterize the topography of the RSF/I_3QGK scaffolds as shown in Fig. 2. Coating of the I_3QGK peptide onto cover glass formed a uniform layer of peptide nanofibers

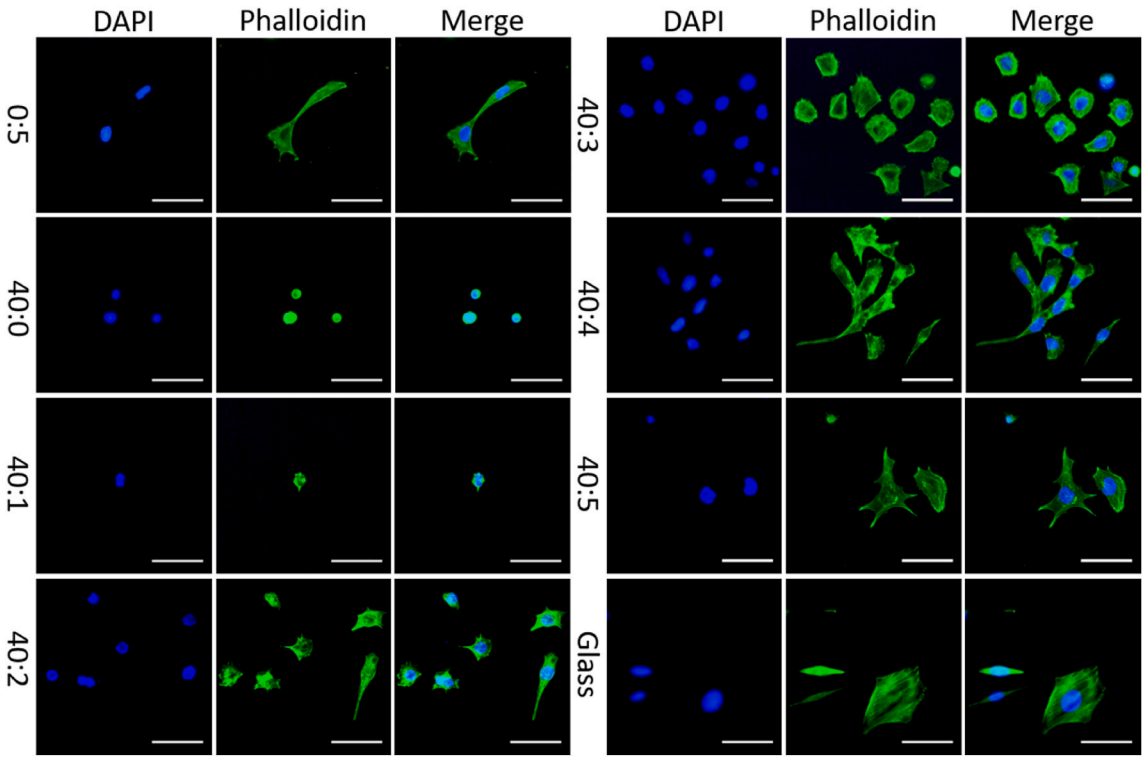

Fig. 4. Fluorescence images of PC12 neuronal cells attached to various RSF/I_3QGK coated surfaces (blue: DAPI staining for nucleus, and green: phalloidin staining for F-actin). Scale bars for all images = 50 μm.

(Fig. 2a), however, the peptide layer can be easily washed away by water (Fig. 2i), making it unsuitable for direct coating on glass surfaces for cell culture applications. Coating of RSF resulted in a smooth layer of silk on glass surface (Fig. 2b), compared to the atomically flat silica surface (Fig. 2h). Ethanol treatment converted Silk I to Silk II structure [65] (rich in β-sheet), making it water insoluble. While the RSF is overall negatively charged [66], coating of the positively charged I_3QGK peptide nanofibers on the top of a silk layer resulted in a strong charge-charge interaction between the silk coating and the peptide material. With increasing concentration of I_3QGK, the amount of nanofibers adhered to the RSF scaffold surface increased and a near full coverage was observed at a concentration of 3 mg/mL (Fig. 2c–f). Further increasing the concentration of I_3QGK resulted in stacking of nanotubes (Fig. 2f and g), which could potentially lead to cell detachment during cell culture.

3.3. Cellular adhesion and viability

The cell adhesion and viability experiments were carried out by live/dead assay on different RSF/I_3QGK coated scaffolds as shown in Fig. 3. Poor PC12 cell attachment was observed on I_3QGK coated glass surfaces compared to RSF/I_3QGK coated surfaces (Fig. 3A). This is assumed to be due to the washing off of I_3QGK nanofibers during cell culture, which resulted in the exposure of the underlying bare glass surface. This result was consistent with the AFM analysis shown in Fig. 2i. Pure RSF coated surfaces also exhibited poor cell attachment due to the lack of cell recognized functional groups and a weak negatively charged surface property (Fig. 3A (b)). However, the samples coated with I_3QGK peptide nanofibers on RSF substrates provided enhanced cell adhesion due to the electrostatic charge-charge interactions between the RSF layer and I_3QGK nanofibers, providing enough positively charged lysine residues on the surface to facilitate cell binding [38]. A significant difference in cell density was observed between I_3QGK (3–5 mg/mL)/RSF and pure RSF (40 mg/mL) coated scaffolds (Fig. 3B, ****$p < 0.0001$), indicating that PC12 neuronal cells have a low bonding affinity on pure RSF (40 mg/mL) substrates. The scaffold surface topography has a significant effect to the cell spreading. In general, with increasing I_3QGK concentration (onto RSF substrates) the number of cells attached onto the surface increased (Fig. 3B), indicating that the higher surface roughness resulted in better cell spreading. However, when the concentration of I_3QGK increased to 5 mg/mL, the number of cells decreased slightly with some areas having no cell attachment (Fig. 3A (g) and Fig. 3B, ***$p < 0.001$). This may result from the detachment of the stacked nanofibers (Fig. 2g) when using a high concentration of peptide solution for surface coating. This means the biomechanical factors also play an important role. When more peptide fibres are on the surface, the binding between some peptide fibres become loose and detachment happened upon the buffer wash after live/dead staining. PC12 cells on bare glass slides showed poor attachment with aggregation (Fig. 3A (h)). The Live/dead assay demonstrated that cells attached on the different concentration ratio (RSF/I_3QGK) coated substrates were ~100% live (green) with no detectable dead cells, indicating that RSF/I_3QGK scaffolds have excellent biocompatibility (Fig. 3C). In contrast, some dead cells (red) were observed on bare glass surfaces. From this it can be assumed that the combination of RSF and I_3QGK provide a good solution for neuronal cell attachment and proliferation. The best I_3QGK concentrations for coating RSF surfaces were seen to be 3–4 mg/mL. The results demonstrate that the I_3QGK peptide nanofibrous scaffolds exhibited a similar efficacy to other previously reported peptide scaffolds for tissue engineering [50,67,68].

3.4. Cell morphology

To investigate cell morphology, cell nuclei and F-actin were stained for neuronal cells attached on the different RSF/I_3QGK coated substrates (Fig. 4). Cell morphology on RSF (40 mg/mL) and RSF/I_3QGK (at a concentration ratio of 40:1) coated substrates showed poor spreading. All cells were round shaped and the number of cells attached on the substrates was very low. Cell morphology on 5 mg/mL I_3QGK coated glass surface (0:5) showed better cell spreading. However, the

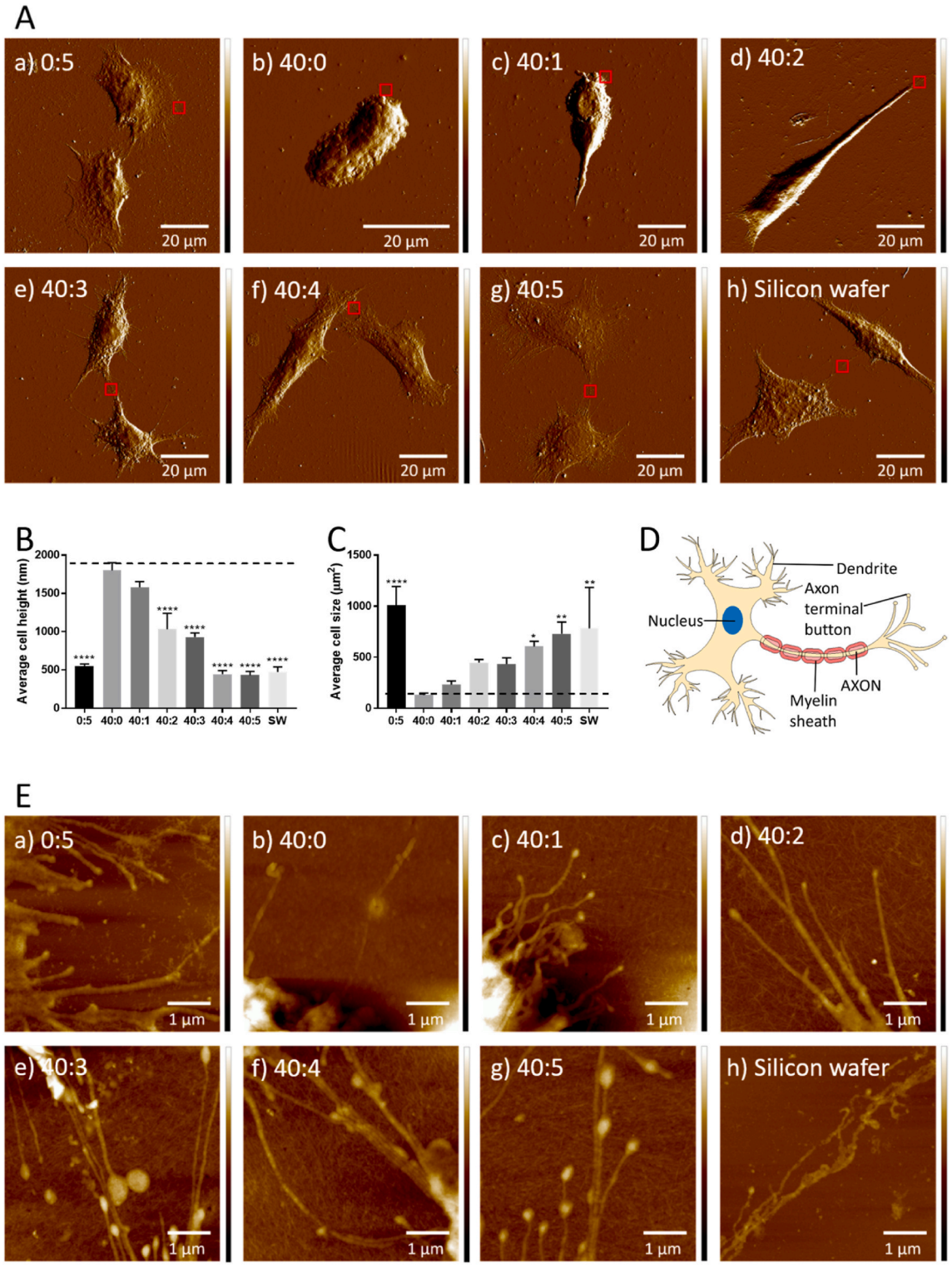

Fig. 5. A, AFM peak force images of PC12 neuronal cells attached to different concentrations of RSF/I_3QGK coated substrates. The concentration ratios of RSF and I_3QGK were: (a) 0:5, (b) 40:0, (c) 40:1, (d) 40:2, (e) 40:3, (f) 40:4, (g) 40:5 and (h) bare silicon wafer. The force set point constant was 30 nN in all images. The areas indicated by the red boxes were scanned and are shown in **E**. Average cell height and size of PC12 cells on various coated samples are shown in **B** and **C**, where 'SW' denotes the bare silicon wafer surface. All values were compared to RSF (40 mg/mL) coated surfaces. ($n \geq 3$; ****$p < 0.0001$; **$p < 0.01$; *$p < 0.05$). **D**, a schematic shows representative morphology of a typical neuron cell. **E**, AFM topographical images (25 μm^2) of the red box areas shown in Fig. 5A. The Z scale (height) bars are 150 nm for all images.

number of cells attached was also low due to the wash off of peptide from the surface. Cell morphology on the RSF/I_3QGK coated scaffolds at the concentration ratios of 40:2, 40:3 and 40:4 showed improved spreading and the number of cells also increased. In contrast the cell attachment on 40:5 ratios and cover glass were in patches, although the spreading was also excellent.

AFM was used to further characterize the morphology of the PC12 neuronal cells adhered to the different RSF/I_3QGK coated substrates

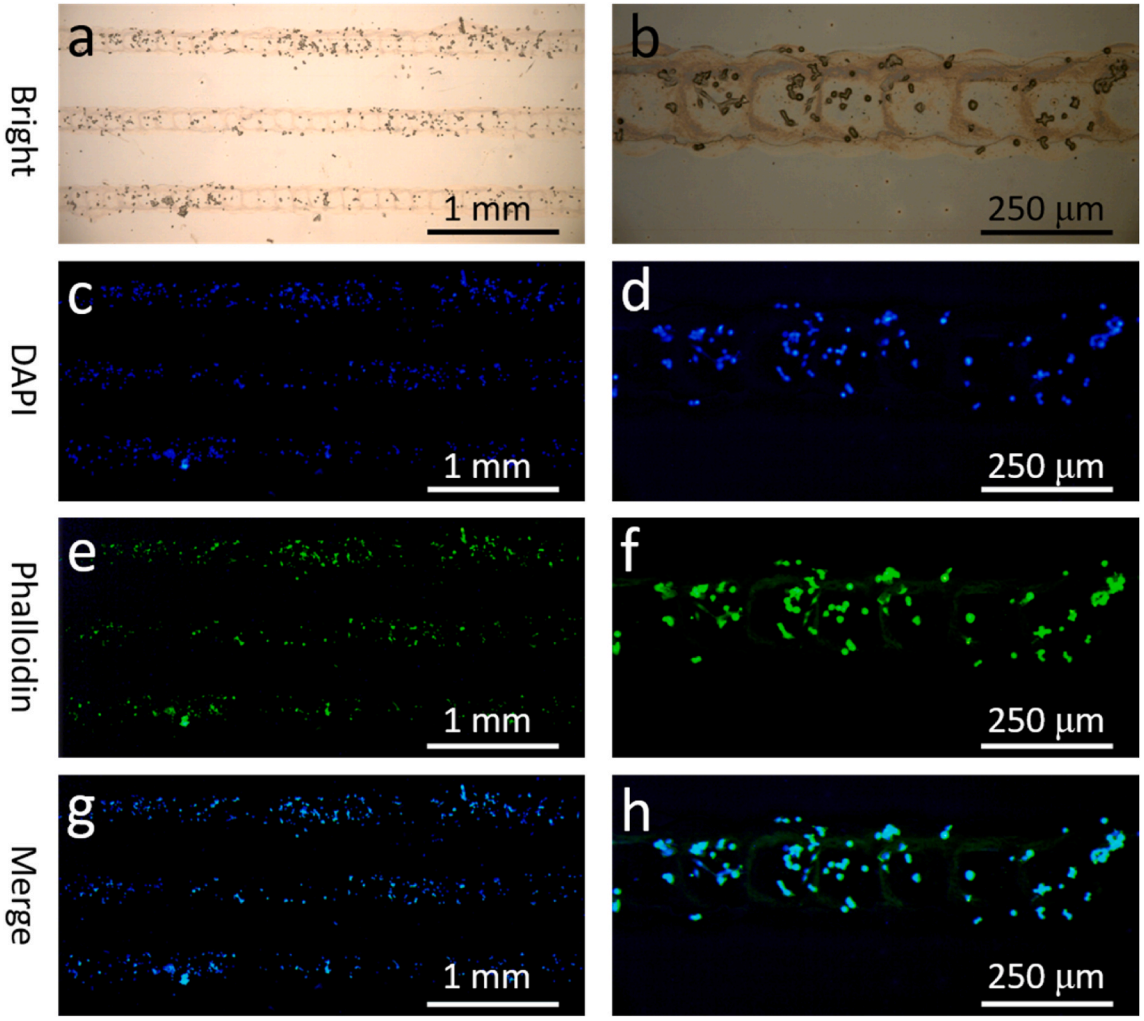

Fig. 6. Inkjet printing of I_3QGK peptide lines (5 layers) on RSF (40 mg/mL) coated surfaces. PC12 neuronal cells only attached on the printed lines. (**a** & **b**) Bright-field microscopy images of printed lines. (**c** & **d**) Fluorescent micrographs of PC12 cells on printed lines (DAPI staining of nuclei). (**e** & **f**) Phalloidin staining of F-actin. (**g** & **h**) are the merged images of c & e, and f & h. For all images, lines were printed with 5 layers of peptides. Scale bars = 1 mm for a, c, e and g and 250 µm for b, d, f and h.

(Fig. 5A and E). On 5 mg/mL I_3QGK coated glass, cell spread out on the glass surface (Fig. 5A (a)). However, as shown in Fig. 5A (b), cells attached to the pure RSF (40 mg/mL) substrate did not spread out, while the cells on I_3QGK coated on RSF samples(Fig. 5A (c)–(g)) started to spread and become elongated onto RSF/I_3QGK coated scaffolds. The process of cell adhesion on a polymer surface can be divided into three phases [11,69]. Cell attachment on pure RSF coated substrate corresponds to phase I, passive cell adhesion. In phase I, cells adhere on coated substrate by physiochemical interactions, including van der Waals, hydrophobic and coulombic forces, and can easily detach [70]. While on the I_3QGK coated RSF substrates, cells have interactions with the positively charged lysine residues as active adhesion. At different concentration ratios (40:1; 40:2; 40:3 and 40:4) of RSF/I_3QGK coated substrates, cells started to spread and become flattened due to integrin binding, which is considered as phase II. At a concentration ratio of 40:5 (RSF/I_3QGK) the cells were fully spread and the cytoskeleton was organized to form focal adhesion, which is known as phase III. Therefore, RSF/I_3QGK coated scaffolds possess highly cell-adhesive properties. With the increasing concentration of I_3QGK used for coating, the cells attachment to the substrate surfaces was enhanced.

The average cell height and size on the different RSF/I_3QGK coated substrates were analysed to further investigate the cell adhesion and spreading (Fig. 5B and C). A steady decrease of the cell height was observed while increasing the peptide concentration for coating. The average height of the cells on RSF coated surface was found around 1800 ± 80 nm while on the 4–5 mg/mL I_3QGK coated substrates the average height was found only 450 ± 40 nm (Fig. 5B, ****$p < 0.0001$), which is very similar to (but slight lower than) that on silicon wafer surfaces. In contrast, the average cell size (footprint) increased gradually with increasing peptide concentration and up to an 8 fold increase was observed at 5 mg/mL (Fig. 5C, ****$p < 0.0001$). The variance of average cell size was high on the 5 mg/mL I_3QGK coated glass and silicon wafer surfaces, indicating the poor uniformity on these surfaces. These results illustrate I_3QGK coated substrates show a better cellular adhesion and spreading than the RSF (40 mg/mL) coated substrates, indicating I_3QGK is an excellent biomaterial for PC12 cell growth.

The morphology of a typical neuron cell (Fig. 5D) includes a nucleus, dendrites, an axon and axon terminal buttons [71]. To further investigate the structure of neurites, the areas within the red boxes on Fig. 5A were scanned by AFM and shown in Fig. 5E. It can be seen from the enlarged AFM morphology images that the dendrites were not well spread on silicon wafer, 0:5 and 40:0 surfaces. In contrast, when increasing the peptide concentration from 1 to -5 mg/mL for the coating, enhanced neurite growth was observed. Terminal buttons can be clearly seen in Fig. 5E (e)–(g). Increasing the I_3QGK concentration for coating resulted in increased length of axons as well as the increased size of the terminal buttons. These results are comparable to those that use ECM

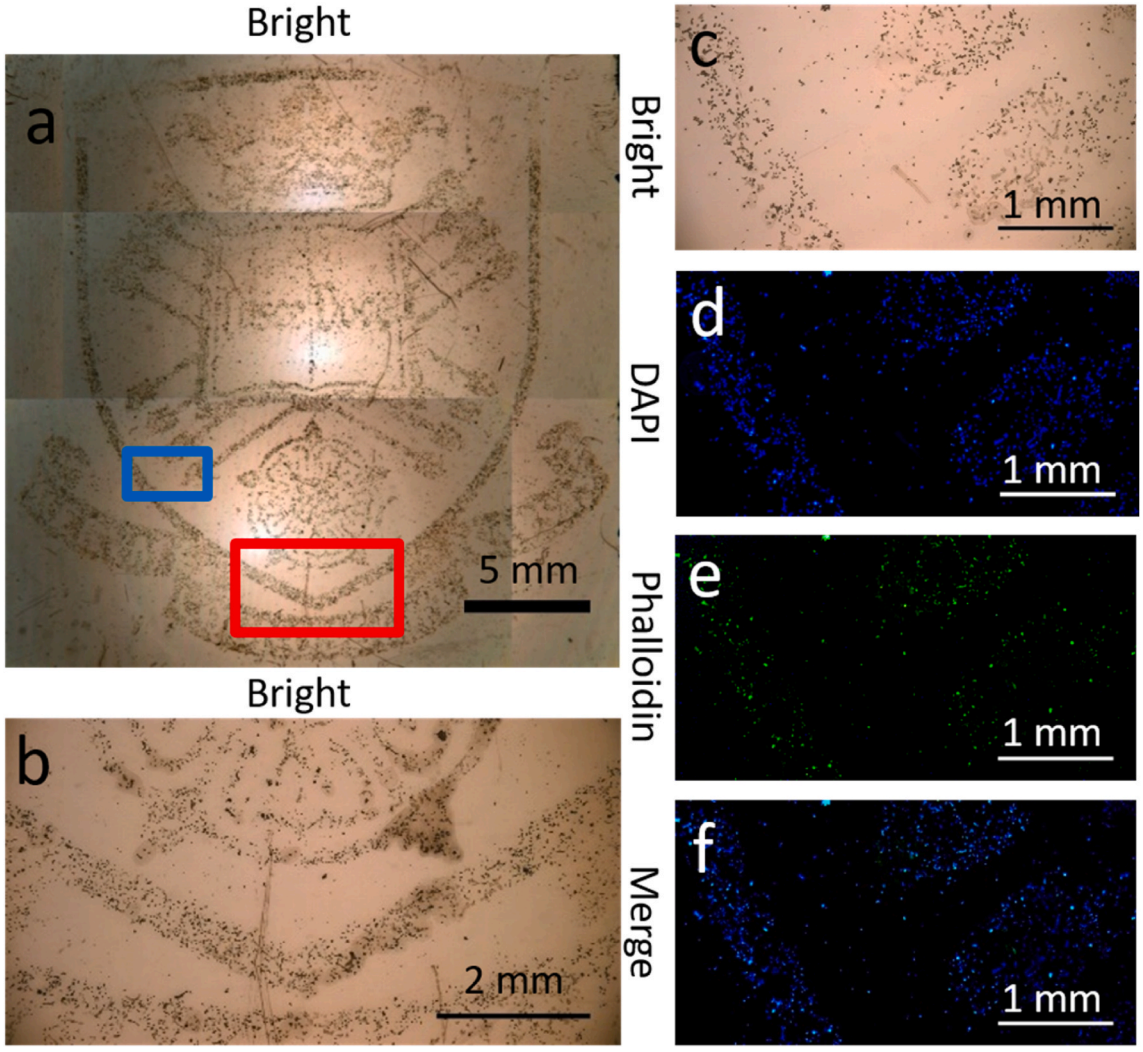

Fig. 7. (**a**) Inkjet-printed University of Sheffield logo (on RSF a coated glass surface) using I_3QGK peptide ink, with PC12 neuronal cells growing along the printed pattern. The red and blue box areas are shown in (**b**) and (**c**), respectively. Fluorescence microscopy images of the printed logo: (**d**) DAPI staining for nuclei. (**e**) Phalloidin staining of F-actin. (**f**) The merged images of (**d**) and (**e**). The logo was printed with 1 layer of peptide (3 mg/mL).

proteins such as collagen for neuron patterning, in which neurite outgrowth was observed due to the interaction of collagen with the cell surface integrins [10]. The close proximity of the axon terminal buttons gives great potential to conduct electrical signals to another axon by a nerve synapse response. Although the cells adhered on glass and silicon wafer surfaces (Fig. 5E (a) and (h)) had long axons, the terminal buttons were not observed. And neurites adhered onto silicon wafers appeared very unhealthy (Fig. 5E (h)). These results strongly indicate that I_3QGK can promote neurite formation. These results are consistent with previously work [54] that I_3QGK nanofibers showed excellent biocompatibility (similar to collagen) and can facilitate rapid and effective hemostasis by gelling the blood and promoting platelet adhesion. It is likely that I_3QGK nanofibers provide a suitable niche for cell attachment and spreading. The amino groups in the peptides serve as ligands for cell surface interactions, similar to that in RGD and poly(L)-lysine [72]. It has been shown that the slope, density and affinity of ligand all had significant effect to the cell attachment and migration [72]. The surfaces coated with different concentrations of I3QGK had different effects to PC12 cell attachment and, spreading, and subsequently affected the development of neuronal phenotype.

3.5. PC12 neuronal cell alignment to micro-patterns produced by inkjet printing

Neuronal cell alignment plays an essential role in axonal regeneration and is a key aspect of nerve tissue engineering [73,74]. Inkjet printing is an emerging technology that can be used to micropattern biological materials in a non-contact fashion therefore, has been employed here to pattern the peptide nanofibers onto RSF coated substrates [60,75–77]. The printed peptides in each layer were uniform at the middle of the droplet footprint. Peptide fibres fully covered the silk substrate (40 mg/mL) after 1 layer printing with an ink concentration at 3 mg/mL (Fig. S2), which is similar to previous results (Fig. 2e). However, the height of each layer on the edge was higher than that in the middle. This is because of the 'coffee ring effect' of the inkjet printing possesses that leads more peptide fibres accumulated on the edge of each footprint [78]. Increasing the number of layers resulted in rougher surface in the middle and higher edges (Fig. S2). PC12 cells showed better attachment on the edge of the printed patterns. (Fig. 6a and b).

Peptide lines (Fig. 6) and more complex structures such as the University of Sheffield logo (Fig. 7) were fabricated by inkjet printing of I_3QGK (3 mg/mL) nanofibers onto RSF (40 mg/mL) coated substrates. As was demonstrated in Fig. 6, PC12 cells only grew along the printed

patterns. With increasing layers, the number of cells attached to printed lines increased (Fig. S3). This indicates that PC12 cells proliferation and attachment onto I_3QGK substrates depends on the amount of peptide nanofibers adhered to the surface. The alignment of cells play a dominant role in cell differentiation, cellular microenvironment and cell-cell interactions and therefore, micro-patterning of cells via inkjet printing of peptides may provide a useful tool for future studies of neuronal cell behaviour such as axonal development [60,74,79]. The live/dead assay (Fig. 3) has demonstrated that the PC12 on the peptide nanofibers showed excellent viability, comparable to that on gelatin methacrylate (GelMA) scaffold [80]. GelMA contains cell recognized peptide RGD, and has been widely used as 3D hydrogel scaffolds in tissue engineering. Recently, Ye et al. [80] reported that GelMA scaffolds fabricated by 3D printing can be used as nerve guidance conduits (NGC) whose aim is regenerate large-gap nerve injuries. Here, peptide I_3QGK has also shown excellent neuronal cell compatibility. Therefore, it has a great potential to be used in the fabrication of NGC in future.

4. Conclusions

In summary, the synthetic peptide I_3QGK can dynamically self-assemble into nanofibers, which can be coated or printed onto RSF scaffolds via charge-charge interactions and improve neuronal cell attachment and differentiation as well as neurite outgrowth. The concentration of the I_3QGK used for coating (which affects the nanofiber coverage) has a significant effect to cell attachment and morphology. We find concentrations between 3 and 4 mg/mL coated on RSF substrates to be the ideal condition for PC12 neuronal cells with best attachment and proliferation. More importantly, it can be used to guide axonal regeneration and promote the growth of axon terminal buttons. In addition, I_3QGK and RSF exhibit low cytotoxicity against PC12 neuronal cells. Inkjet printing is capable of depositing functional peptide nanofiber inks into complex patterns and facilitating cell alignment for tissue engineering applications [81], providing a way for further analysis of *in vitro* cellular functions [82] such as axonal development.

Declaration of competing interest

The authors declare that they have no known competing financial interests or personal relationships that could have appeared to influence the work reported in this paper.

Acknowledgements

The authors would like to thank the EPSRC (EP/N007174/1 and EP/N023579/1), Royal Society (RG160662 and IE150457) and Jiangsu specially-appointed professor program for support.

Appendix A. Supplementary data

Supplementary data to this article can be found online at https://doi.org/10.1016/j.pnsc.2020.09.007.

References

[1] D. Singh, A.J. Harding, E. Albadawi, F.M. Boissonade, J.W. Haycock, F. Claeyssens, Acta Biomater. 78 (2018) 48–63.
[2] H.S. Koh, T. Yong, C.K. Chan, S. Ramakrishna, Biomaterials 29 (26) (2008) 3574–3582.
[3] P. Sensharma, G. Madhumathi, R.D. Jayant, A.K. Jaiswal, Materials science & engineering C, Materials for biological applications 77 (2017) 1302–1315.
[4] E. Schnell, K. Klinkhammer, S. Balzer, G. Brook, D. Klee, P. Dalton, et al., Biomaterials 28 (19) (2007) 3012–3025.
[5] X. Du, Y. Wang, L. Yuan, Y. Weng, G. Chen, Z. Hu, Colloids Surf. B Biointerfaces 122 (2014) 79–84.
[6] X. Li, R. You, Z. Luo, G. Chen, M. Li, J. Mater. Chem. B 4 (17) (2016) 2903–2912.
[7] Q. He, H.G. Sudibya, Z. Yin, S. Wu, H. Li, F. Boey, et al., ACS Nano 4 (6) (2010) 3201–3208.
[8] B. Kang, J. Shin, H.-J. Park, C. Rhyou, D. Kang, S.-J. Lee, et al., Nat. Commun. 9 (1) (2018) 5402.
[9] M. Théry, J. Cell Sci. 123 (24) (2010) 4201–4213.
[10] V. Malkoc, D. Gallego-Perez, T. Nelson, J.J. Lannutti, D.J. Hansford, J. Micromech. Microeng. 25 (12) (2015) 125001.
[11] L. Chen, C. Yan, Z. Zheng, Mater. Today 21 (1) (2018) 38–59.
[12] D. Ren, Y. Xia, J. Wang, Z. You, Sensor. Actuator. B Chem. 188 (2013) 340–346.
[13] Y. Wang, Z. Xu, L.C. Kam, P. Shi, Advanced Healthcare Materials 3 (2) (2014) 214–220.
[14] C. Wu, X. Zhu, T. Man, P.-S. Chung, M.A. Teitell, P.-Y. Chiou, Lab Chip 18 (20) (2018) 3074–3078.
[15] Y. Xia, G.M. Whitesides, Annu. Rev. Mater. Sci. 28 (1) (1998) 153–184.
[16] M.K. Gupta, S.K. Khokhar, D.M. Phillips, L.A. Sowards, L.F. Drummy, M.P. Kadakia, et al., Langmuir 23 (3) (2007) 1315–1319.
[17] A. Martinez-Rivas, G.K. Gonzalez-Quijano, S. Proa-Coronado, C. Severac, E. Dague, Micromachines 8 (12) (2017).
[18] L. Mecozzi, O. Gennari, R. Rega, L. Battista, P. Ferraro, S. Grilli, Macromol. Biosci. 17 (3) (2017).
[19] Y. Nahmias, D.J. Odde, Nat. Protoc. 1 (5) (2006) 2288–2296.
[20] S.M. Naseer, A. Manbachi, M. Samandari, P. Walch, Y. Gao, Y.S. Zhang, et al., Biofabrication 9 (1) (2017) 015020.
[21] C.C.W. Tse, S.S. Ng, J. Stringer, S. MacNeil, J.W. Haycock, P.J. Smith, International Journal of Bioprinting 2 (2016).
[22] F.-J. Xu, Chin. Chem. Lett. 30 (12) (2019) 2051–2052.
[23] X. Cui, T. Boland, D.D. D'Lima, M.K. Lotz, Recent Pat. Drug Deliv. Formulation 6 (2) (2012) 149–155.
[24] C. Zhang, Y. Zhang, H. Shao, X. Hu, ACS Appl. Mater. Interfaces 8 (5) (2016) 3349–3358.
[25] W. Song, M. Muthana, J. Mukherjee, R.J. Falconer, C.A. Biggs, X. Zhao, ACS Biomater. Sci. Eng. 3 (6) (2017) 1027–1038.
[26] C. Correia, S. Bhumiratana, L.P. Yan, A.L. Oliveira, J.M. Gimble, D. Rockwood, et al., Acta Biomater. 8 (7) (2012) 2483–2492.
[27] M. Zhu, K. Wang, J. Mei, C. Li, J. Zhang, W. Zheng, et al., Acta Biomater. 10 (5) (2014) 2014–2023.
[28] W. Zhang, L. Chen, J. Chen, L. Wang, X. Gui, J. Ran, et al., Advanced healthcare materials 6 (10) (2017).
[29] Y. Qi, H. Wang, K. Wei, Y. Yang, R.-Y. Zheng, I. Kim, et al., Int. J. Mol. Sci. 18 (3) (2017) 237.
[30] S.L. Jackman, C.H. Chen, S.N. Chettih, S.Q. Neufeld, I.R. Drew, C.K. Agba, et al., Cell Rep. 22 (12) (2018) 3351–3361.
[31] U.-J. Kim, J. Park, C. Li, H.-J. Jin, R. Valluzzi, D.L. Kaplan, Biomacromolecules 5 (3) (2004) 786–792.
[32] Y. Tamada, Biomacromolecules 6 (6) (2005) 3100–3106.
[33] C.B. Borkner, M.B. Elsner, T. Scheibel, ACS Appl. Mater. Interfaces 6 (18) (2014) 15611–15625.
[34] F. Zhang, B. Zuo, Z. Fan, Z. Xie, Q. Lu, X. Zhang, et al., Biomacromolecules 13 (3) (2012) 798–804.
[35] M.E. Kinahan, E. Filippidi, S. Köster, X. Hu, H.M. Evans, T. Pfohl, et al., Biomacromolecules 12 (5) (2011) 1504–1511.
[36] M.M. Jacobsen, D. Li, N. Gyune Rim, D. Backman, M.L. Smith, J.Y. Wong, Sci. Rep. 7 (2017) 45653.
[37] B. Panilaitis, G.H. Altman, J. Chen, H.-J. Jin, V. Karageorgiou, D.L. Kaplan, Biomaterials 24 (18) (2003) 3079–3085.
[38] Y.H. Kim, N.S. Baek, Y.H. Han, M.-A. Chung, S.-D. Jung, J. Neurosci. Methods 202 (1) (2011) 38–44.
[39] D. Lam, H.A. Enright, J. Cadena, S.K.G. Peters, A.P. Sales, J.J. Osburn, et al., Sci. Rep. 9 (1) (2019) 4159.
[40] K.M. Koss, M.A. Churchward, A.T. Nguyen, J.Y. Yager, K.G. Todd, L.D. Unsworth, Acta Biomater. 35 (2016) 127–137.
[41] S.F. Badylak, Semin. Cell Dev. Biol. 13 (5) (2002) 377–383.
[42] J.W. Lee, K.Y. Lee, Colloids Surf. B Biointerfaces 152 (2017) 36–41.
[43] Y.H. Yang, Z. Khan, C. Ma, H.J. Lim, L.A. Smith Callahan, Acta Biomater. 21 (2015) 55–62.
[44] W.H. Kim, H.W. Schnaper, M. Nomizu, Y. Yamada, H.K. Kleinman, Canc. Res. 54 (18) (1994) 5005–5010.
[45] C.M.M. Motta, K.J. Endres, C. Wesdemiotis, R.K. Willits, M.L. Becker, Biomaterials 218 (2019) 119335.
[46] Z. Ma, M. Kotaki, R. Inai, S. Ramakrishna, Tissue Eng. 11 (1–2) (2005) 101–109.
[47] S. Zhang, Nat. Biotechnol. 21 (2003) 1171.
[48] X. Zhao, F. Pan, H. Xu, M. Yaseen, H. Shan, C.A. Hauser, et al., Chem. Soc. Rev. 39 (9) (2010) 3480–3498.
[49] E. Genové, C. Shen, S. Zhang, C.E. Semino, Biomaterials 26 (16) (2005) 3341–3351.
[50] R.G. Ellis-Behnke, Y.-X. Liang, S.-W. You, D.K.C. Tay, S. Zhang, K.-F. So, et al., Proc. Natl. Acad. Sci. U. S. A 103 (13) (2006) 5054–5059.
[51] M.E. Davis, J.P.M. Motion, D.A. Narmoneva, T. Takahashi, D. Hakuno, R.D. Kamm, et al., Circulation 111 (4) (2005) 442–450.
[52] Y. Yanlian, K. Ulung, W. Xiumei, A. Horii, H. Yokoi, Z. Shuguang, Nano Today 4 (2) (2009) 193–210.
[53] E.C. Wu, S. Zhang, C.A.E. Hauser, Adv. Funct. Mater. 22 (3) (2012) 456–468.
[54] C. Chen, Y. Zhang, R. Fei, C. Cao, M. Wang, J. Wang, et al., ACS Appl. Mater. Interfaces 8 (28) (2016) 17833–17841.
[55] T. Wang, G. Qu, Y. Deng, J. Shang, Z. Feng, F. Yang, et al., Chin. Chem. Lett. 30 (12) (2019) 2368–2374.
[56] H.Y. Wang, Y.Q. Zhang, Sci. Rep. 4 (2014) 6182.
[57] R.H. Westerink, A.G. Ewing, Acta Physiol. 192 (2) (2008) 273–285.
[58] A. Levi, J. Eldridge, B. Paterson, Science 229 (4711) (1985) 393–395.

[59] S. Aznar-Cervantes, A. Pagan, J.G. Martinez, A. Bernabeu-Esclapez, T.F. Otero, L. Meseguer-Olmo, et al., Materials science & engineering C, Materials for biological applications 79 (2017) 315–325.
[60] J. Guo, S. Ling, W. Li, Y. Chen, C. Li, F.G. Omenetto, et al., Adv. Funct. Mater. 28 (19) (2018) 1800228.
[61] X. Zhao, F. Pan, S. Perumal, H. Xu, J.R. Lu, J.R.P. Webster, Soft Matter 5 (8) (2009) 1630.
[62] D.A. Gregory, Y. Zhang, P.J. Smith, X. Zhao, S.J. Ebbens, Small 12 (30) (2016) 4048–4055.
[63] H. Xu, Y. Wang, X. Ge, S. Han, S. Wang, P. Zhou, et al., Chem. Mater. 22 (18) (2010) 5165–5173.
[64] Q. Wang, X. Zhang, J. Zheng, D. Liu, RSC Adv. 4 (48) (2014) 25461.
[65] A. Gd, Z. Yu, J. Sp, Z. Xiubo, J. ES. Small. 12 (30) (2016) 4048–4055.
[66] X. Wang, J.A. Kluge, G.G. Leisk, D.L. Kaplan, Biomaterials 29 (8) (2008) 1054–1064.
[67] H. Cao, T. Liu, S.Y. Chew, Adv. Drug Deliv. Rev. 61 (12) (2009) 1055–1064.
[68] G.A. Silva, C. Czeisler, K.L. Niece, E. Beniash, D.A. Harrington, J.A. Kessler, et al., Science 303 (5662) (2004) 1352–1355.
[69] A.A. Khalili, M.R. Ahmad, Int. J. Mol. Sci. 16 (8) (2015) 18149–18184.
[70] T. Okano, N. Yamada, M. Okuhara, H. Sakai, Y. Sakurai, Biomaterials 16 (4) (1995) 297–303.
[71] A. Ghahari, J.D. Enderle, ISRN Ophthalmol 2014 (2014) 406210.
[72] E-j Lee, E.W.L. Chan, W. Luo, M.N. Yousaf, RSC Adv. 4 (60) (2014) 31581–31588.
[73] V. Guenard, N. Kleitman, T. Morrissey, R. Bunge, P. Aebischer, J. Neurosci. 12 (9) (1992) 3310–3320.
[74] Y. Li, G. Huang, X. Zhang, L. Wang, Y. Du, T.J. Lu, et al., Biotechnol. Adv. 32 (2) (2014) 347–365.
[75] S.V. Murphy, A. Atala, Nat. Biotechnol. 32 (8) (2014) 773–785.
[76] H. Tao, B. Marelli, M. Yang, B. An, M.S. Onses, J.A. Rogers, et al., Adv. Mater. 27 (29) (2015) 4273–4279.
[77] J.A. Phillippi, E. Miller, L. Weiss, J. Huard, A. Waggoner, P. Campbell, Stem Cell. 26 (1) (2008) 127–134.
[78] P. He, B. Derby, Advanced Materials Interfaces 4 (22) (2017) 1700944.
[79] K. Kawaguchi, R. Kageyama, M. Sano, Nature 545 (7654) (2017) 327–331.
[80] W. Ye, H. Li, K. Yu, C. Xie, P. Wang, Y. Zheng, et al., Mater. Des. 192 (2020) 108757.
[81] C.J. Lee, P. Huie, T. Leng, M.C. Peterman, M.F. Marmor, M.S. Blumenkranz, et al., Arch. Ophthalmol. 120 (12) (2002) 1714–1718.
[82] R. Singhvi, A. Kumar, G. Lopez, G. Stephanopoulos, D. Wang, G. Whitesides, et al., Science 264 (5159) (1994) 696–698.